

## **Appendix A**

# **Growth of diamond nanocrystals by pulsed laser ablation of graphite in liquid**

### **§ A.1 Introduction**

The synthesis of diamond has been pursued ever since the French chemist Antoine Laurent Lavoisier discovered that diamond was a form of crystalline carbon [1]. The first report describing successful diamond synthesis using high-pressure, high-temperature (HPHT) methods was published in 1955 [2], in which diamond was crystallised from metal-solvated carbon at pressures and temperatures in the region of 55,000 atmospheres and  $\sim 1800^{\circ}\text{C}$ . Since then, extensive worldwide research efforts have been made to synthesis diamond due to its extraordinary physical properties. These include the following [3]:

- Exceptional hardness
- Wide spectral range transparency
- Chemical inertness
- High thermal conductivity
- Highest atomic number density
- Highest elastic modulus
- Very low coefficient of expansion
- Low coefficient of friction, comparable to Teflon
- Biological compatibility
- When doped becomes semiconducting

- Good electrical insulator
- Very resistant to chemical corrosion
- Exhibits low or ‘negative’ electron affinity

Given these many notable properties it is not surprising to learn that diamond has already found uses in many variant applications such as heat sinks, abrasives [4], and wear-resistant coatings for cutting tools [5]. It is also possible to envisage that diamond has huge potential as an engineering material in many other applications. For example, if diamond could be used as a substrate for microelectronic circuits, thermal management would be easier, considering dissipation of the heat generated is a major problem during device operation. Moreover, if electronic grade (containing extremely low levels of impurities and defects) diamond could be produced, and doped, it would be possible to create microelectronics out of diamond. The high carrier mobility [6], wide band gap and thermal stability of diamond means these devices would be able to operate faster, and under much more extreme conditions than silicon based devices. However, progress in implementing many such ideas has been restricted by the scarcity of naturally occurring diamond. It has therefore long been desired by scientists to devise methods to synthesise diamond in the laboratory.

Among the various diamond deposition methods, LP-PLA is a relatively newcomer. Very recently, Yang *et al.* [7] converted hexagonal graphite into cubic diamond crystals via intermediate rhombohedral graphite using this technique. It is believed that nanocrystalline and ultrananocrystalline diamonds have potentially a large number of applications [8, 9]. Hence, controlling the size of nanocrystalline diamond and the higher probability of graphite to diamond transition are essential for the experimental design. Compared with ablating at a gas-solid interface, LP-PLA can create a higher pressure, higher temperature, and higher density plasma plume at the liquid-solid interface, combined with a simple experimental setup and room temperature, atmospheric pressure operation. Nanocrystalline diamond has also been produced by LP-PLA using a graphite target along with water or acetone as the liquid medium [10,11]. The main conclusions achieved by these researchers were that OH groups formed from the oxygen-containing liquids were etching non-diamond carbon species from the surface, thereby allowing diamond to form

preferentially. Thus, the OH was thought to be playing a role analogous to that of atomic hydrogen in conventional diamond CVD [12]. However, it was recently shown [13] that diamond particles could be made using LP-PLA in cyclohexane, suggesting that OH is not necessary for diamond formation.

Although LP-PLA is becoming established as a route to diamond nanoparticle synthesis, a detailed description of the fundamental processes occurring in the laser-solid-liquid system is still lacking. To this end, we shall present results about LP-PLA nanocrystal diamond growth from graphite/water, together with a study of the optical emission from the plume.

## **§ A 2 Experimental details**

The ablation apparatus used has been described elsewhere [14] and in Chapter 3. The solid and liquid system was a graphite target (Testbourne Ltd., 99.99%) and 5-10 ml of deionised water, which covered the target to depth of 5 mm. Two types of cell was used, please refer Chapter 3.3.12 section for more details. The incident 532 nm Nd:YAG laser beam was directed by a prism and then focused using a 50 mm-focal-length biconvex lens through the liquid layer and onto the surface of the target to produce a spot size of ~0.5 mm diameter. The laser output had a pulse length of 15 ns and energy of approximately 125 mJ per pulse, which is sufficient to easily obtain breakdown in water. The laser fluence at the target surface was ~28 J cm<sup>-2</sup>. The ablation was performed for times of 0.5-1 h.

After irradiation, the liquid often appeared slightly coloured (usually pale yellow) due to the suspension of nanoparticles. This suspension was pipetted onto a microscope slide or TEM grids. The TEM grids (Agar Scientific) were SiO<sub>2</sub>-coated to ensure that the elemental fingerprint of the sample was not confused with that from the grid. SAED, HRTEM with EDX analysis were employed to identify the compositional, structural and morphology information of the prepared materials. Laser Raman spectroscopy (Renishaw 2000, excitation wavelength 325 nm) was used to study the bonding configuration. Optical emission spectroscopy (OES) was

used to monitor the composition of the plasma accompanying the LP-PLA process (see Chapter 3.3.12 section for further details).

### **§ A 3 Results and discussion**

The TEM analysis revealed that the ablated product contained a mixture of amorphous carbon and graphite from the target, plus a small amount of faceted crystalline nanostructures. EDX spectra indicated the presence of only C, Si and O in the area being studied (Si and O were from the TEM grid). Figure A.1(a) shows some typical faceted nanocrystals which were found at the edges of larger pieces of graphite, following 30 min ablation of graphite in water. The size of the crystallites (Figure A.1(b)) increased to ~100 nm when the reaction time doubled to 1 h. Similar morphology for diamond crystals is commonly seen in gas-phase CVD deposition [15,16]. A typical SAED ring pattern from the nanocrystals is shown in Figure A.1(c), and the lattice plane spacings for the four inner rings were analysed using a standard computer program [17]. They corresponded well to the {110}, {111}, {220} and {300} planes of diamond [18, 19], as can be seen in Table A.1. The observed lattice planes (Figure A.1(d)) in HRTEM are consistent with the (111) planes of crystalline diamond with an interplanar distance of 2.06 Å [20]. The above analyses are all consistent with a hexagonal diamond structure, similar to that reported in refs.[18,19].

The Raman spectra of the (a) target graphite bulk and (b) nanocrystals are shown in Figure A.2. After laser irradiation, the spectrum from the graphite target shows only the G band at 1568 cm<sup>-1</sup> arising from ordered graphite [21]. The Raman spectrum from the nanoparticles also showed the G band (but with a slight shift to 1565 cm<sup>-1</sup>) which could indicate the presence of bond-angle disorder. A weak peak at 1333 cm<sup>-1</sup> is also seen as the fingerprint for sp<sup>3</sup>-bonded C in diamond [21]. The relative size of the G band to that of the diamond peak is not unexpected given the low yield of diamond nanoparticles in the graphite background.

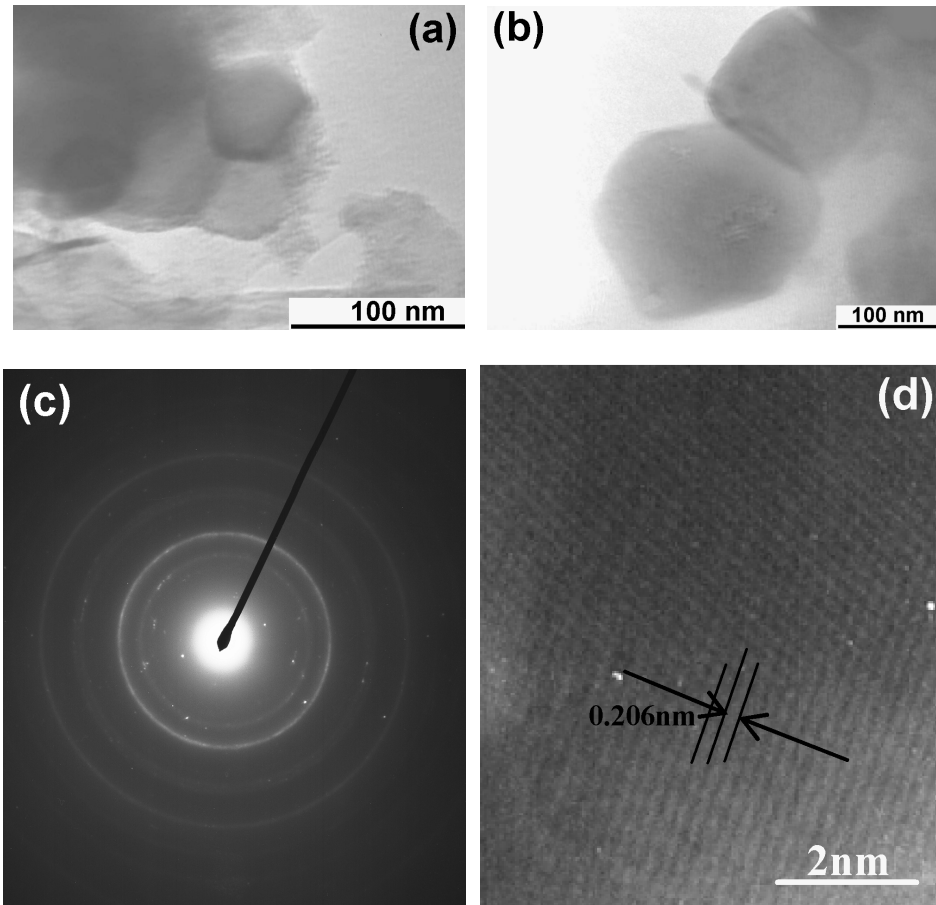


Figure A.1 TEM images of samples produced by LP-PLA of a graphite target in water (laser fluence at 125 mJ per pulse) for durations of: (a)  $t = 0.5$  h, (b)  $t = 1$  h. (c) A typical SAED pattern taken from (a). (d) HRTEM lattice planes corresponding to diamond (111) planes.

Table A.1 The lattice  $d$ -spacings of the four inner rings calculated from the SAED data (Figure A.1(c)) with comparison to those for diamond and graphite [18,19].

| $d_{\text{experiment}} / \text{\AA}$ | $\langle hkl \rangle_{\text{diamond}}$ | $d_{\text{diamond}} / \text{\AA}$ | $d_{\text{graphite}} / \text{\AA}$ |
|--------------------------------------|--|-----------------------------------|------------------------------------|
| 2.534                                | $\langle 110 \rangle$                  | 2.522                             | 3.355                              |
| 2.034                                | $\langle 111 \rangle$                  | 2.059                             | 2.034                              |
| 1.283                                | $\langle 220 \rangle$                  | 1.261                             | 1.232                              |
| 1.186                                | $\langle 300 \rangle$                  | 1.189                             | 1.157                              |

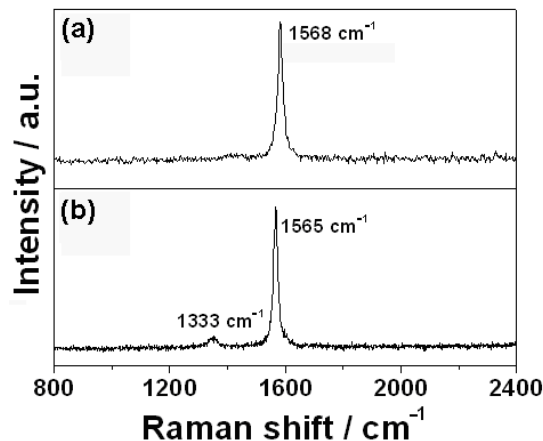


Figure A.2 Raman spectra of (a) the graphite target and (b) the nanocrystals formed by LP-PLA of graphite in water at 125 mJ laser fluence and 1 h ablation time.

Figure A.3 shows wavelength-resolved emission spectra of the ablation plume induced by 532 nm laser excitation. Emission from atomic C and C<sup>+</sup> is observed as a direct result of the ablation process. But the presence of atomic H and O shows that the water is also being dissociated in the PLA process, either directly by interaction with the high energy laser, or indirectly as a result of reactions with the high kinetic energy ejected atoms and particles in the plume. Such plume reactions have been seen previously during PLA of graphite in vacuum or in gaseous nitrogen or argon, backgrounds [23,24,22]. The presence of the strong peaks from atomic H is interesting, since H is believed to be necessary for the growth of diamond in conventional gas-phase CVD methods [12]. Peaks from atomic H were also seen previously during diamond growth from LP-PLA of graphite in cyclohexane [13]. This suggests that atomic H maybe a common reagent necessary in both LP-PLA and CVD diamond growth, and that the growth mechanism may therefore be similar in both systems.

Figure A.4 shows an example image of the ablation plume at the graphite-water interface following frame-capture by a video camera. Figure A.4(a) shows the geometry of the open cell before the laser pulse occurs. Figure A.4(b) is an example of one of the emission plumes seen during ablation. There were considerable shot-to-shot variations in the shape and size of the emission, resulting from non-

uniformities in the target surface, bubbles within the liquid, and droplets ejected into the air. In Figure A.4(b), numerous small droplets can be seen being ejected from the cell, one of which (top left) has passed directly through the laser beam and scattered/re-emitted light.

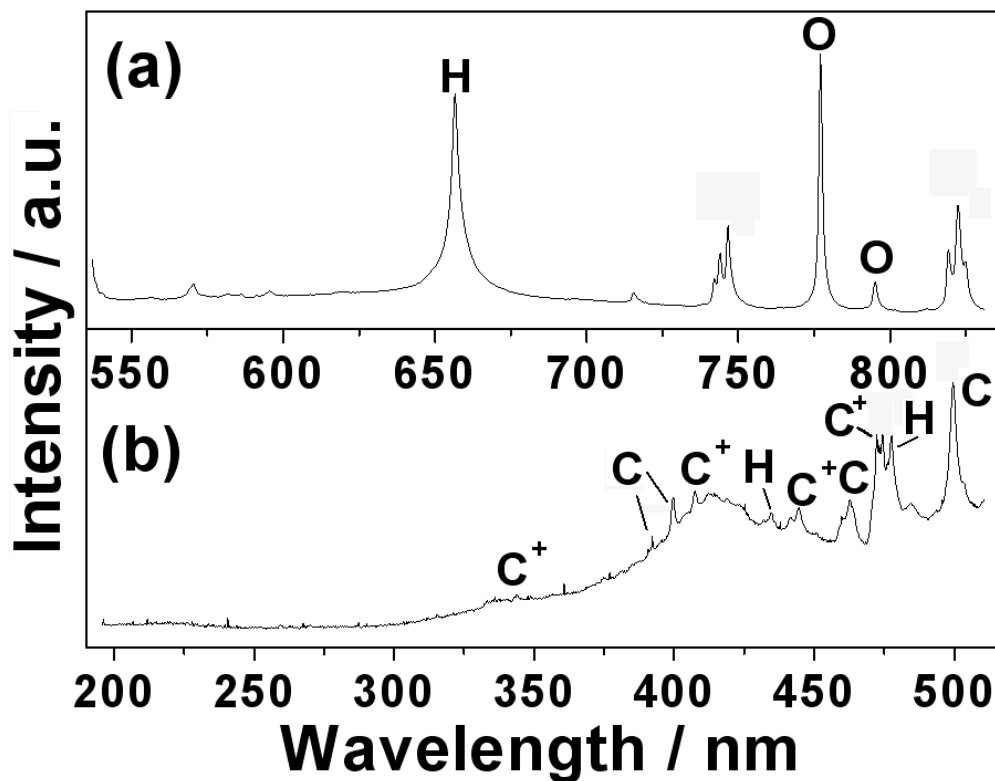


Figure A.3 Wavelength-dispersed optical emission spectra of the plume accompanying 532 nm LP-PLA of graphite in water. The spectrum has been split into two halves, (a) and (b), either side of the intense reflected laser peak at 532 nm (not shown). The features have been assigned to atomic H, O, and C, and  $C^+$  ions (using literature values [23,24] as reference). The features around 740 and 825 nm have not been assigned but are possibly due to  $N_2$ .

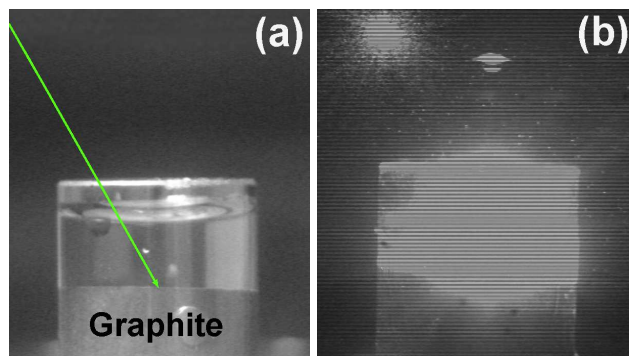


Figure A.4 (a) Photograph of the open cell showing the position of water and graphite target, as well as the direction of the laser beam (directed at an oblique angle to try to reduce the chance of water splashing onto the prism). (b) Image immediately following the laser pulse, showing the bright emission from the ablation plume. Top left shows emission from a droplet which has passed directly through the laser beam and scattered/re-emitted light.

Figure A.5 shows two typical frame images captured from the video when using a 656 nm filter to observe only the emission from atomic H. It can be seen in Figure A.5(a) that the H emission arises from two regions along the path of the laser pulse, one within the water close to the target, and the other in the air a few mm above the water surface. This suggests that the time-averaged emission shown previously (Figure A.4) is actually a result of at least two separate processes. In the water region, excited H atoms are being created either as a result of (i) direct laser interaction causing breakdown of the water, or (ii) reaction between water and energetic ablated C atoms, ions or particles ejected from the surface, or (iii) the collapse of cavitation bubbles [25]. The presence of atomic H in the liquid phase near to the graphite surface is consistent with the idea that H is required for graphite-to-diamond conversion. Excited H atoms are also created in the air region, again as a result of processes (i) or (ii). Figure A.5(b) shows another captured image displaying a smaller secondary emission region within the water. These secondary plasma regions sometimes occurred within the liquid, or in the air, or in both simultaneously, and highlight the shot-to-shot variability of the process.

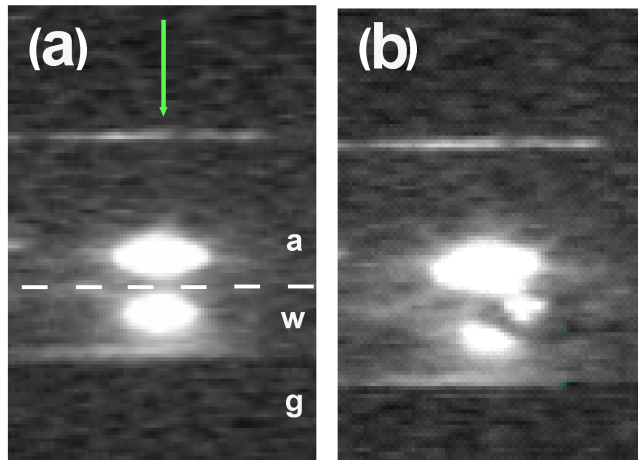


Figure A.5 Two i-CCD images of the total emission resulting from 532 nm, 15 ns PLA of graphite in water recorded using an H Balmer (656 nm) filter in front of the camera. The white dashed line shown in (a) indicates the position of the interface between the water, w, and air, a, with graphite target, g, below. The bright horizontal line near the top of each image is the top edge of the cell window through which the laser (illustrated by the arrow) passes. Each laser pulse produced a slightly different image, of which most resembled (a) with bright plasma balls in both the water and the air directly above the surface of the target. However, sometimes the images showed secondary plasma balls, such as in (b), probably due to the ejection of larger graphitic particulates from the target interacting with and being excited by the laser pulse.

#### **§ A 4 Conclusions**

We have demonstrated that nanocrystalline diamond particles can be formed using LP-PLA. TEM/SAED/Raman analyses confirm that the ablated material is consistent with a faceted diamond phase. Optical emission spectroscopy shows that the ablation process produces two plasma regions, one confined into the liquid and one in the air just above the liquid surface. Emission from atomic H within these regions is consistent with the idea that H is required for diamond growth, even in an

aqueous medium. To gain further insight into this mechanism, an obvious extension of this work would be to perform time resolved studies using a fast gated CCD, and to increase the spatial resolution so that the emission from the air and water regions could be imaged separately.

However, from analysis of the composition of the ablation product, we estimate that the yield of nanodiamond particles is only about 5%, with the remainder being graphitic particles ejected from the target. Thus, development of a suitable separation procedure would be required to increase the efficiency of this process, and this would be essential if LP-PLA were to be used as a commercially viable method of producing nanodiamond. Possible routes might be oxidation and removal of the unwanted graphitic particles using hot, strong acids, and/or separation methods using high-speed centrifuge followed by filtration techniques.

## **Bibliography**

- [1] Lavoisier A L, *Memoire Acedemie des Science*, 1772, 564.
- [2] Bundy F P, Hall H T, Strong H M, Wentorf R H, *Nature*, 1955, **176**, 51.
- [3] Field J E, *Properties of Natural and Synthetic Diamond*, Academic Press, London, 1992.
- [4] Davies G, *Diamond*, Adam Hilger, Bristol, 1984.
- [5] Yoder M N, *Diamond Films and Coatings*, Noyes Publications, 1993.
- [6] Isberg J, Hammersberg J, Johansson E, Wikstrom T, Twitchen D J, Whitehead A J, Coe S E, Scarsbrook G A, *Science*, 2002, **297**, 1670.
- [7] Yang G W, Wang J B, *Appl. Phys. A*, 2001, **72**, 475.
- [8] Gerbi J E, Auciello O, Birrell J, Gruen D M, Alphenaar B W, Carlisle J A, *Appl. Phys. Lett.*, 2003, **83**, 2001.
- [9] Bundy F P, Bassett W A, Weathers M S, Hemley R J, Mao H K, Goncharov A F, *Carbon*, 1996, **34**, 141.
- [10] Wang J B, Zhang C Y, Zhong X L, Yang G W, *Chem. Phys. Lett.*, 2002, **361**, 86.
- [11] Wang J B, Yang G W, *J. Phys.: Condens. Matt.* 1999, **11**, 7089.
- [12] May P W, *Phil. Trans. R. Soc. Lond. A*, 2000, **358**, 473.
- [13] Pearce S R J, Henley S J, Claeysens F, May P W, Hallam K R, Smith J A, Rosser K N, *Diam. Relat. Maters.*, 2004, **13**, 661.

- [14] Yang L, May P W, Yin L, Smith J A; Rosser K N, *Diamond Relat. Mater.*, 2007, **16**, 725.
- [15] Ashfold M N R., May P W, Rego C A, Everitt N M, *Chem. Soc. Rev.*, 1994, **23**, 21.
- [16] Partridge P G, Ashfold M N R, May P W, Nicholson E D, *J. Mater. Sci.*, 1995 **30**, 3973.
- [17] Lábár J L, Frank In L, Ciampor F (Eds.), *Proceedings of EUREM*, July 2000, vol. III, **12**, Brno, p.1379.
- [18] Yang G W, Wang J B, Liu Q X, *J. Phys.: Condens. Matter*, 1998, **10**, 7923.
- [19] Yagi T, Utsumi W, Yamakata M, Kikegawa T, Shimomura O, *Phys. Rev. B*, 1992, **46**, 6031.
- [20] Vereshchagin A L, Yur'ev G S, *Inorganic Mater.*, 2003, **39**, 247.
- [21] Filik J, *Spectroscopy Europe*, 2005, **17**, 10.
- [22] Fuge G M, Rennick C J, Pearce S R J, Henley S J, May P W, Ashfold M N R, *Diamond Relat. Mater.*, 2003, **12**, 1049.
- [23] Claeysens F, Ashfold M N R, Sofoulakis E, Ristoscu C G, Anglos D, Fotakis C, *J. Appl. Phys.* , 2002, **91**, 6162.
- [24] Fuge G M, Ashfold M N R, Henley S J, *J. Appl. Phys.* , 2006, **99**, 014309.
- [25] Yavas O, Schilling A, Bischof J, Boneberg J, Leiderer P, *Appl. Phys. A*, 1997, **64**, 331.